Correlating Nanomorphology with Charge-Transport Anisotropy in Conjugated-Polymer Thin Films

By *Yi-Fang Huang, Chan-Wei Chang, Detlef-Matthias Smilgies, U-Ser Jeng, Anto Regis Inigo, Jonathon David White,* Kang-Chuang Li, Tsong-Shin Lim, Tai-De Li, Hsiang-Yun Chen, Show-An Chen, Wen-Chang Chen,* and *Wun-Shain Fann*

Dedicated to the memory of Professor W. S. Fann.

Flexible plastic devices such as cell phone displays and smart tags comprised of thin-film light-emitting diodes (LEDs) or field-effect transistors (FETs) as well as photovoltaics based on amorphous conjugated polymers promise low-cost fabrication and low energy consumption due to solution processing.[1] While carrier type and mobility (μ) are key parameters in describing such semiconducting materials, these quantities are not necessarily directionally independent in devices based on thin films. Indeed, charge-transport anisotropy in crystalline and liquid-crystalline semiconductors is a well-established phenomenon.[2] For more amorphous materials, experiments over the past few decades have also found that the mobility laterally in the thin-film-transistor (TFT) geometry (μ_{FE}) is up to four orders of magnitude greater than that measured vertically in a diode configuration.[3] By spin-coating and drop casting poly[2-methoxy-5-(2′-ethyl-hexyloxy)-1,4-phenylene vinylene] (MEH-PPV) films from two different solvents, we show that differences in measured mobility are due to an interfacial layer of several nanometers at the film/substrate interface formed via spin-coating, having a higher electron density assisted by local chain alignment parallel to the substrate.

Over the years, numerous explanations have been proposed for the anisotropy in the measured values of mobility. Delannoy et al. suggested the existence of traps operative under the conditions of the time-of-flight (TOF) experiment but not under those that hold during TFT operation results in a reduced mobility in the vertical direction.[4] Dodabalapur et al.[5] suggested that increased mobility in the TFT configuration may be also due to the much higher value of electric field in this configuration as compared to the diode configuration. More recently, Tanase et al. and Pasveer et al.[6,7] have argued that this difference results from a strong dependence of the mobility on charge-carrier density, while Meng et al.[8] have argued strongly against this interpretation, proposing that the effect, at least for MEH-PPV-containing aggregates, is the result of an alignment of aggregates (or crystallites) during aging.

Related to the issue of morphology, considerable additional work has been published concerning poly(3-hexyl thiophene) (P3HT) films. Sirringhaus et al.[9] showed that for spin-coated films, crystallites are generally oriented with their (100)-axis normal to the substrate. However, the combination of low regioregularity and low molecular weight (M_w) results in the axis being rotated parallel to the substrate. They suggested that this is the mechanism responsible for the two orders of magnitude differences in TFT mobilities reported in the literature. More recent X-ray diffraction (XRD) studies by Kline et al. revealed that for spin-coated films there exists a thin layer at the film-substrate interface with properties different from the bulk.[10] For low-molecular-weight

[*] Prof. J. D. White
Department of Electrical Engineering
Yuan Ze University
Neili, Taoyuan 320 (Taiwan)
E-mail: whitejd@xiaotu.com
Dr. Y. F. Huang, Dr. A. R. Inigo, K. C. Li, Prof. W. S. Fann
Institute of Atomic and Molecular Sciences
Academia Sinica
P. O. Box 23-166
Taipei 106 (Taiwan)
C. W. Chang, Prof. W. C. Chen, Prof. W. S. Fann
Institute of Polymer Science and Engineering
National Taiwan University
Taipei 106 (Taiwan)
Dr. D.-M. Smilgies
Cornell High Energy Synchrotron Source (CHESS)
Wilson Laboratory, Cornell University
Ithaca, NY 14853 (USA)
Dr. U. S. Jeng
National Synchrotron Radiation Research Center
Hsinchu 300 (Taiwan)
Prof. T. S. Lim
Department of Physics
Tunghai University
Taichung 407 (Taiwan)
Dr. T. D, Li, Prof. W. S. Fann
Department of Physics
National Taiwan University
Taipei 106 (Taiwan)
H. Y. Chen[+], Prof. S. A. Chen
Department of Chemical Engineering
National Tsing Hua University
Hsinchu 300 (Taiwan)
[+] Present address: Department of Chemistry
Texas ASH University
College Station, TX 77483 (USA)

DOI: 10.1002/adma.200803341

polymers, the orientation of crystals (and hence FET mobility) in this interfacial layer was found to be dependent on surface treatment whereas this is not the case for high-molecular-weight polymers.[10] In an extreme case, Yang et al.[11] demonstrated that film structure (for both spin and drop-cast films) could be changed drastically when M_w was reduced to 3.6 kDa.

In our study, we extend this work to more glassy polymers. In particular, we investigate thin films of low-polydispersity, high-molecular-weight polymers of MEH-PPV, a derivative of the well-studied polymer poly(phenylenevinylene) (PPV)—a polymer generally considered to exhibit much less crystal structure than P3HT.[12] First, we demonstrate that the mobilities measured in the diode and FET configurations for these three films are inversely correlated, indicating that some directional inhomogeneity must be present in the film itself. Secondly, synchrotron X-ray radiation is used to probe the microstructure and texture, revealing both local short-range packing of MEH-PPV chains parallel and adjacent to the substrate in all films and an additional global thin high-density layer (~5 nm thick) most strongly pronounced in films spin-coated from chlorobenzene (CB), in which charge-transport anisotropy is greatest. Finally, we propose that the primary reason for the anisotropy in measured mobility values is this solvent-dependent high-electron-density layer lying along the interface, which aids hole movement in the FET geometry. A secondary effect appears to be local, short-range ordered packing: in the diode configuration, holes must travel perpendicular to the chain packing, while in the FET geometry holes move parallel to the polymer backbone.

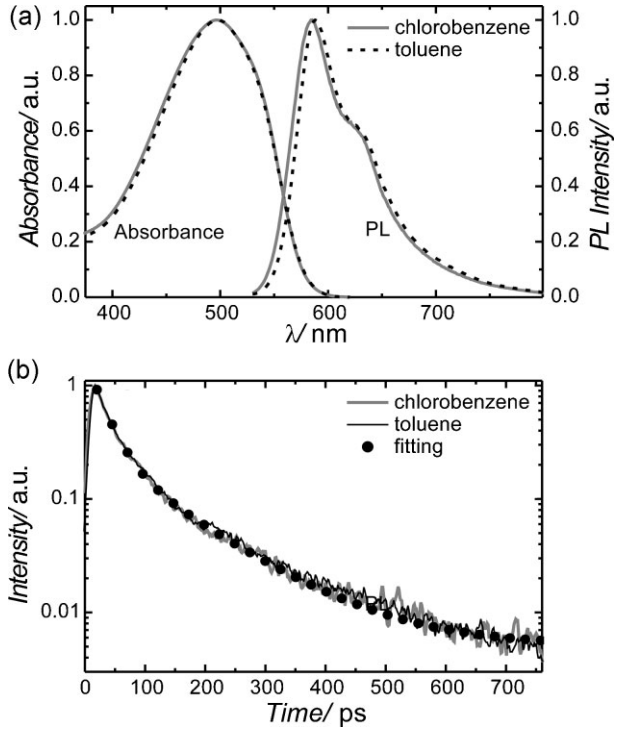

Figure 1. a) UV–vis absorbance and far-field PL emission spectra (λ_{excite} = 510 nm) of MEH-PPV thin films spin-coated from CB and TL solutions. b) Time-resolved PL decay. (λ_{excite} = 460 nm, $\lambda_{detection}$ = 590). Closed circles show the two exponential fitting of the time-resolved PL (τ_1 = 25 ps, τ_2 = 120 ps, χ^2 = 0.99858).

Figure 1a presents the UV–vis absorbance and the photoluminescence emission spectra of the spin-coated films of MEH-PPV (M_w ~880 kDa, δ = 1.11) prepared from toluene (TL) and CB solutions. Both films show similar absorbance and PL spectra (excluding a slight solvochromatic shift), indicating similar optical properties. The time-resolved PL (Fig. 1b) indicates that the decay times are also similar, as is the photoluminescence excitation spectra (Supporting Information Fig. S5). This similarity of optical properties indicates that the strength of interchain interactions in the two spin-coated films is of a similar magnitude. Thus, any difference in mobility between the two spin-coated films is not the result from differences in the strength of interchain interactions, as commonly observed in other systems.[13] In contrast, the spectrum of the drop cast film is more intense in the red region, indicating that interchain interactions play a greater role in it relative to the spin-coated films. As the hole-trapping state does not depend on solvent,[14] we can conclude that any observed differences in charge transport between the two spin-coated films must be due to other morphological factors.

Charge mobility perpendicular to the substrate was measured using the transient electroluminescence (TrEL) technique for the spin-coated films, and the TOF technique for drop-cast films, while mobility parallel to the substrate was measured using the bottom-contact FET geometry. Figure 2 summarizes our mobility measurements as a function of electric field for all devices. For the spin-coated films, the horizontal (FET configuration) mobilities (μ_{FE}) are approximately three orders higher than the vertical (diode configuration, μ_{diode}) values (see Supporting Information Fig. S6 and S8 for typical raw data). For drop-cast films both horizontal and vertical mobilities are the same order of magnitude. The horizontal mobility for the film spun from CB is a factor of four greater than for films spun from TL, in distinct contrast to transport in the vertical direction, where the TL films exhibited an order of magnitude greater mobility than those spun from CB.

As a part of the difference in absolute values may be due to different measurement techniques (see discussion in ref. [15], Supporting Information), we define a mobility anisotropy parameter $\eta = \mu_{FE}/\mu_{diode}$ to allow the results to be compared. The values for the three films are $\eta_{CB\text{-}spin} \sim 10^4$, $\eta_{TL\text{-}spin} \sim 10^2$, and $\eta_{CB\text{-}drop} \sim 1$. This said, we also believe that the absolute values of

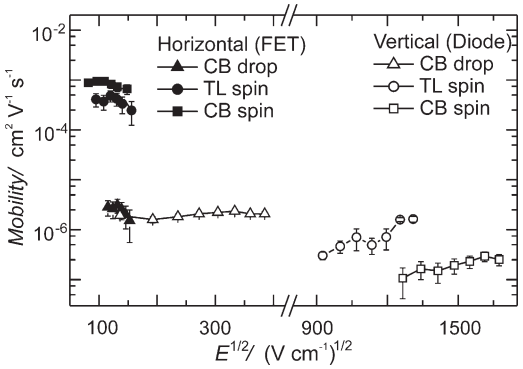

Figure 2. Summary of the field-dependent hole mobilities measured in FET and diode configurations plotted as a function of the square of the electric field for the three films.

anisotropy for a single solvent are meaningful numbers, as we note that Meng et al.[8] have used the SCLC technique to measure both vertical and horizontal mobilities for films spun from MEH-PPV dissolved in chloroform (a good solvent similar to CB). Their reported anisotropy for the spin-coated films was $\eta_{\text{CB-spin}} \sim 10^3$–$10^4$, while mobility was found to be isotropic ($\eta_{\text{CB-drop}} = 1$) in drop cast films, in remarkable agreement with the values for our CB cast films.

The observed anisotropy clearly indicates that the differences in mobilities measured in the FET and diode configurations are not predominantly an effect of the different charge-carrier densities in the two devices as previously suggested,[6,7] but rather due to a structural or morphological anisotropy induced by the spin-coating process. If the higher mobilities observed in the FET configuration relative to the diode configuration in spin-coated films was primarily a charge-carrier effect, one would expect that the anisotropy factor would be similar for the two spin-coated films. One would also expect that the solvent that gives the highest mobility in one configuration would also give the highest mobility in the other configuration, in contrast to the observed experimental data. We thus conclude that a structural or morphological anisotropy exists in the spin-coated films. The isotropic charge transport in drop-cast films indicates the morphological anisotropy responsible for this phenomena is weak or absent in drop-cast films (spin speed = 0), suggesting that this anisotropy is induced by the spin-coating process.

The structure of the three films was investigated using X-ray scattering techniques. The key experimental results are summarized in Figure 3. Figure 3b *inset* displays a grazing-incidence wide-angle X-ray scattering (GI-WAXS) pattern of a spin-coated MEH-PPV film prepared from CB. The meridional reflection (perpendicular to the substrate) at scattering vector $Q = 15.2\,\text{nm}^{-1}$ suggests a vertical inter-backbone packing with a d-spacing of 0.41 nm (consistent with the value obtained by XRD in Fig. 6b of ref. [16]), while the backbone chains remain parallel to the substrate.[9,17] The weaker equatorial reflection (parallel to the substrate) at scattering vector $Q = 10.0\,\text{nm}^{-1}$ (corresponding to a d-spacing of 0.63 nm) stems from the backbone repeat units of MEH-PPV. The strong arc in the upper-left corner and an adjacent weak scattering ring are due to the indium tin oxide (ITO) substrate layer. On the molecular level, all three films show very similar results.

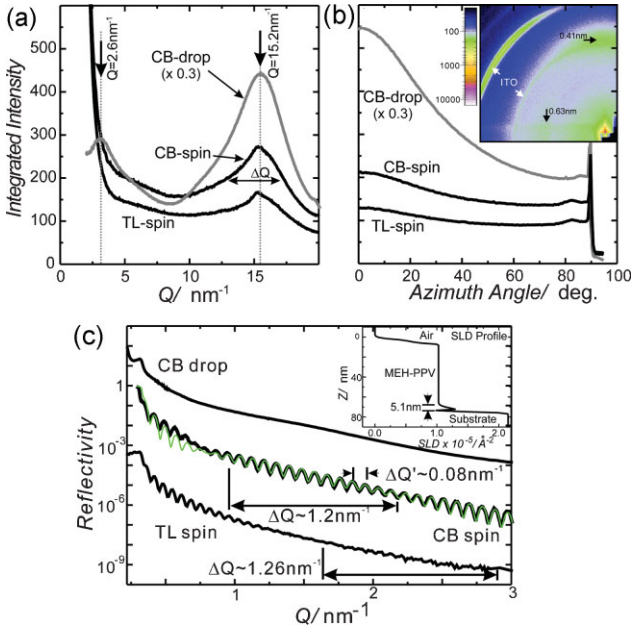

Figure 3. Comparison of the morphology of thin films based on X-ray measurements. GI-WAXS data for the three films integrated the a) radial and b) azimuthal directions. (b-Inset) GI-WAXS pattern of CB spin-coated film. c) XRR of the three (free standing) films along with the calculated pattern based on the two-layer scattering-length density (SLD) profile shown in the bottom-inset. $\Delta Q'$ indicates the period of Kiessig fringes and ΔQ their modulation period.

All three angle-integrated radial scans (Fig. 3a) reveal a broad diffuse peak centered at $Q \sim 15\,\text{nm}^{-1}$ corresponding to the backbone ordering. The sharp little peaks superimposed on it are due to an ITO-powder ring (see Fig. 3b *inset*). The width of this broad peak at $Q \sim 15\,\text{nm}^{-1}$ ($\Delta Q \sim 4\,\text{nm}^{-1}$) corresponds to an average domain size of 1.4 nm, as derived by the Scherrer formula, and taking into account a resolution of $0.4\,\text{nm}^{-1}$. Hence the backbone order extends only over about three lattice constants, confirming that the polymer film is essentially amorphous. However, the azimuth scans at $Q = 15.2\ \text{nm}^{-1}$(Fig. 3b) reveal a preferential alignment of the backbone chains parallel to the surface, although the spread of $\pm 30^\circ$ is quite extended. The maximum at 0°corresponds to the backbone chains being parallel to the surface. Overall, the scattering from the sample is smooth and unstructured. Hence, formation of aggregates of higher degree of order (or crystallinity) inside the film can be excluded. Note that the peaks at approximately 85 and 90° are the Yoneda peaks of the ITO substrate and the film itself: they do not indicate another preferentially oriented phase. The results of the Scherrer and texture analysis are summarized in detail in the Supporting Information (Fig. S9 and Table S1.)

In the classic literature, substrate effects have been widely ignored, and only in recent studies, with authors having more of a surface-science background, more attention has been paid to the substrate. For example, in the P3HT system, there is considerable effect of surface treatment, when spin-coating low molecular weight P3HT.[10] In order to address this issue, we have repeated some of our X-ray measurements using hexamethyldisilazane (HMDS)-coated Si wafers as substrates. These GI-WAXS results are consistent with the results quoted in the paper (see Supporting Information Fig. S10a).

The Bragg reflection, due to side-chain ordering, with d-spacing of 2.4 nm along the film normal should have appeared around $2.6\,\text{nm}^{-1}$ (ref. [12]), but is only weakly seen in the radial scan of the drop-cast film (denoted by an arrow and dotted line in Fig. 3a). In the spin-coated films, this signal is so weak that it cannot be detected due to intense diffuse scattering in the incident plane. Hence, lamella formation seems to be kinetically suppressed in both spin-coated films, which were thinner and thus dried faster. Lamella formation in the drop-cast film, while observable, is still much weaker than in thermally annealed films (see Supporting Information Fig. S10 and ref. [12]).

Figure 3c presents the X-ray reflectivity (XRR) data for the three films cast on the HMDS-coated oxide layer of a silicon wafer with black lines. The XRR of the spin-coated films are characterized by

high-frequency fringes modulated by a lower-frequency oscillation. The high-frequency Kiessig fringes ($\Delta Q'$) reflect the film thickness (~88 nm for CB, ~90 nm for TL). Their extended observability indicates the films are flat and of low roughness. The low-frequency modulation (ΔQ) points to an additional structure within the spin-coated films with a thickness of ~5 nm. In comparison, the reflectivity profile of the drop-cast film is smooth and structureless. Kiessig fringes were not resolved due to the large film thickness (~3400 nm).

For this low-frequency modulation, there are several possible explanations: alternating layers of high and low electron density,[15] a layer of higher electron density at the film/substrate interface, or a layer of higher or lower electron density at the film/air interface. Each of the above density profiles were used as input into Parratt32 XRR simulation software.[18] Attempts to fit with alternating layers of high and low density reproduced the modulation, but either predicted the existence of Bragg peaks, which were not observed experimentally (Fig. S11b of Supporting Information), or required the use of unrealistic values of the electron density. Assuming a thin layer at the film/air interface reproduced the fast thickness oscillations of the reflectivity curve, however, it was not possible to reproduce the low-frequency modulation (Fig. S11a of Supporting Information). The best fit was obtained by dividing the 88 nm film into an 83 nm layer with the MEH-PPV bulk density on top of a ~5 nm layer of slightly higher density (~10%) at the film/substrate interface (Fig. 3 bottom, red line). Figure 3 bottom-inset shows the variation in electron density across the film based on the Parratt32 simulation results. The above results indicate that a thin high-electron-density layer (~5 nm thick) seems to form at the interface between the thin film and the substrate, and that the strength of this effect is solvent dependent.

Attempts were made to fit the TL data, but no significant difference in the quality of fit between a single- and double-layer model was found. The above results indicate that i) a thin high-electron-density layer (~5 nm thick) may form at the interface between the thin film and the substrate, ii) the strength of this effect is solvent dependent, but is iii) film thickness and spin-speed independent (Supporting Information Fig. S12).

In summary, the GI-WAXS data from all three types of samples show a very similar degree of ordering on the molecular scale. However, differences are seen in the XRR data with the existence of a ~5 nm layer of slightly higher electron density at the film/substrate interface for CB-spun films. While most clearly seen in the CB-spun films, a similar less-pronounced interfacial layer may exist for all spin-coated films studied. While such a thin layer is unlikely to affect transport in a diode structure significantly, in an FET structure carriers are confined to within a few nanometer of the SiO_2 interface.[19] The measured carriers (lateral) may then be largely confined within this 5 nm high-electron-density layer, in which apparently movement is easier, resulting in an increased mobility relative to the bulk. A possible explanation would be a higher degree of chain ordering at the interface.

The mechanism by which these two spin-coated films, despite similar optical properties, exhibit different morphologies resulting in vastly different charge-transport mobilities is an interesting problem. It is possible that the vapor pressures of the two solvents play a role. At 20 °C, the vapor pressure of TL (22 mm Hg) is more than twice that of CB (9 mm Hg). This higher vapor pressure of TL leaves less time for the polymer to self-organize in the spin-coated film as compared to CB.

In conclusion, the large directional anisotropy in charge mobility observed in diode and FET measurements in essentially amorphous MEH-PPV thin films is not due to differences in charge-carrier density, trapping, or electric-field effects. Rather, it is the result of inherent structural anisotropy induced in the spin-coating process. While GI-WAXS data implies that the MEH-PPV backbone chains are closely packed and preferentially ordered parallel to the surface, the fact that this ordering is evident in all films indicates that, although it is an attractive candidate, it is a secondary and not the primary driving force for the observed charge-transport anisotropy. Rather, the mobility orders of magnitude higher in the horizontal direction than in the vertical direction seems to be primarily due to the high-density layer found in the XRR data.

This finding has crucial implications on the device level, as it suggests that by controlling the microstructure, mobility in a diode or solar-cell geometry could be increased by over three orders of magnitude in a nominally amorphous system. For example, in solar cells the rather low hole mobility of the polymer phase as compared to the electron mobility of the fullerene limits both device thickness and energy extraction. Numerical simulations[20] show that increasing hole mobility up to the level of electron mobility would allow thicker devices, thus increasing device efficiency up to 11%. Our work shows that such an increase may be possible as current limits to mobility may be the result of morphology rather than a fundamental property of the polymer being investigated, not only for relatively ordered systems, such as P3HT,[9,10] but also for amorphous systems, such as the ruthenium complex $[Ru(bpy)_3]^{2+}(PF_6-)^2$, where bpy is 2,2′-bipyridine and its analogs.

We have shown that local structure can be correlated with device performance parameters, such as electron or hole transport. While it is well known that surface chemistry and solvents effect the mobility of P3HT films, this work extends that work to more-amorphous or glassy polymers,[12] showing that despite a material being nominally amorphous, processing and surface effects may introduce molecular alignment, which may enhance or diminish electronic properties in a directionally dependent manner. The synergy between preparation procedures and surface-sensitive characterization methods shows the promise to significantly expand the knowledge database for the deliberate design of devices with tailored properties.

Experimental

MEH-PPV (M_w ~880 kDa, $\delta = 1.11$), synthesized via the Gilch method [21,22], was dissolved at 5 mg mL^{-1} in either CB or TL, and maintained in a dark, N_2 atmosphere prior to casting. Spin-coating (drop-casting) was used to form ~100 nm (~4000 nm) films of MEH-PPV. After deposition, films were placed in an inert atmosphere for 6 h. The remaining solvent, along with any adsorbed oxygen, was removed by storing the samples in high vacuum for another 12 h. All processing was done at room temperature. Since defect density and trap states are known to play significant roles in hole mobility, the same batch of MEH-PPV was used to prepare all films.

Charge mobility perpendicular to the substrate was measured using the TrEL technique for the spin-coated films and the TOF technique for drop-cast films, while that parallel to the substrate was measured using the bottom-contact FET geometry. In the case of TrEL, a thin layer of

PEDOT-PSS was first coated onto precleaned ITO-coated glass prior to the spin-coating of MEH-PPV. After solvent evaporation, an electrode (Al, 0.5 mm^2 for TrEL; Au, 4 mm^2 for TOF) was evaporated through a shadow mask to define the active area of the diode structure. For TOF measurements, the transit time (t_{tr}) was determined from the characteristic break in the logarithmic current–time plot. Drift mobility (μ_d) was calculated as $\mu_d = L/t_{tr}E$ where L is the device thickness and E is the applied electric field [15]. For TrEL measurements, devices were placed in a cryostat under dynamic high-vacuum of 10^{-6} torr (1 torr = 133.32 Pa) for 12 h prior to measurement. Electrical excitation was achieved by rectangular electrical pulses generated by a home-made pulse generator (10 ns in rise time, 10 Hz in frequency, variable pulse width up to 60 μs). EL was detected using a photomultiplier (Hamamatsu R955) placed on top of the glass window of the cryostat and recorded using digital-storage oscilloscope (Tektronix TDS 744A). Since in this device configuration charge transport is hole dominated, it was assumed that only holes are moving toward the Al electrode, at which point they combine with electrons emitting light. The delay between applied voltage and the onset of EL (t_d) is thus approximately equal to the transit time for holes to travel across the device. The hole mobility, $\mu(E)$, was then calculated from $\mu(E) = L/t_dE = L^2/t_dV$, where L is the device thickness, E the electric field across the sample, and V is the applied voltage [15].

Horizontal mobility was measured using the bottom-contact FET geometry (see Supporting Information Fig. S7). The SiO_2 surface (thickness = 200 nm; capacitance (C_i) = 17 nF cm^2) of the (phosphorus) n^{++} doped ($\sim 2 \times 10^{18}$) silicon wafer was first cleaned by standard RCA-1 cleaning method [23] followed by a mixed solution of hydrogen sulfuric acid and hydrogen peroxide (3:1 v/v), and subsequently modified by adding a monolayer of HMDS. Au (thickness = 90 nm) was evaporated through a shadow mask to define the source and drain electrodes. The width (W) and length (L) of the resulting channel were 1.5 mm and 30 μm, respectively. Finally, the MEH-PPV solution was deposited as discussed above. The electrical characteristics of the device were measured in the dark under ambient conditions using a Keithley 4200 semiconductor analyzer. Mobility was then obtained with relationship:

$$I_d = \frac{WC_i}{2L}\mu_s\left(V_g - V_t\right)^2 \rightarrow \mu_s = \frac{2L}{WC_i}\frac{I_d}{\left(V_g - V_t\right)^2} \text{ for } V_d \geq V_g$$

where V_g, V_t, and V_d are the gate, threshold and drain voltages, respectively, and I_d is the drain current. The field-dependent mobility was derived from the slope of the square root of current ($I_d^{1/2}$) versus gate voltage (V_g) in the saturation regime (Supporting Information Fig. S7b, note that at saturation, $V_d = V_g - V_t$).

Morphological information was obtained from GI-WAXS and XRR measurements on films deposited on ITO-coated glass and hexamethyldisilazane (HMDS)-treated oxidized silicon substrates. GI-WAXS measurements were performed at the D1 station of Cornell High Energy Synchrotron Source (CHESS), Cornell University, USA, which provides 10^{12} photons mm^{-2} sec^{-1} at a photon wavelength of $\lambda = 1.2$ Å. Samples were illuminated at an incident angle of $\sim 0.2^\circ$ and the scattered X-ray photons were detected with a charge-coupled decice (CCD)-type area detector [24]. Data were processed using Fit2D analysis software [25]. XRR measurements were performed using the 8-circle diffractometer at the wiggler beamline BL17B of the National Synchrotron Radiation Research Center (NSRRC) in Taiwan, using an X-ray beam of $\lambda = 1.240$ Å. Data were recorded with a point detector ranging from $Q = 0.1$–4.5 $Å^{-1}$ and covering six orders of magnitude. Data were fitted with various layer models using the Parratt32 software [18].

Acknowledgements

We express our thanks to Kevin D. O'Neil and Oleg A. Semenikhin, who helped with the AFM images shown in the Supporting Information. CHESS is supported by the NSF & NIH/NIGMS via NSF award DMR-0225180. This research is supported by grants NSC no. 96-2752-E-007-007-PAE, NSC no. 96-2752-E-007-008-PAE, and NSC no. 95-2112-M-155-001 from the National Science Council of the Republic of China. Supporting Information is available online from Wiley InterScience or from the author.

Received: November 13, 2008
Revised: February 17, 2009
Published online:

[1] G. Malliaras, R. Friend, *Phys. Today* **2005**, *58*, 53.
[2] I. O. Shklyarevskiy, P. Jonkheijm, N. Stutzmann, D. Wasserberg, H. J. Wondergem, P. C. M. Christianen, A. P. H. J. Schenning, D. M. de Leeuw, Z. Tomovic, J. S. Wu, K. Mullen, J. C. Maan, *J. Am. Chem. Soc.* **2005**, *127*, 16233.
[3] H. S. Nalwa, *Handbook of Organic Conductive Molecules and Polymers*, Wiley, Chichester, New York **1997**.
[4] P. Delannoy, G. Horowitz, H. Bouchriha, F. Deloffre, J. L. Fave, F. Garnier, R. Hajlaoui, M. Heyman, F. Kouki, J. L. Monge, P. Valat, V. Wintgens, A. Yassar, *Synth. Met.* **1994**, *67*, 197.
[5] A. Dodabalapur, L. Torsi, H. E. Katz, *Science* **1995**, *268*, 270.
[6] C. Tanase, E. J. Meijer, P. W. M. Blom, D. M. de Leeuw, *Phys. Rev. Lett.* **2003**, *91*, 216601.
[7] W. F. Pasveer, J. Cottaar, C. Tanase, R. Coehoorn, P. A. Bobbert, P. W. M. Blom, D. M. de Leeuw, M. A. J. Michels, *Phys. Rev. Lett.* **2005**, *94*, 206601.
[8] H. F. Meng, B. L. Chen, K. C. Tzeng, S. F. Horng, *Appl. Phys. Lett.* **2006**, *88*, 023505.
[9] H. Sirringhaus, P. J. Brown, R. H. Friend, M. M. Nielsen, K. Bechgaard, B. M. W. Langeveld-Voss, A. J. H. Spiering, R. A. J. Janssen, E. W. Meijer, P. Herwig, D. M. de Leeuw, *Nature* **1999**, *401*, 685.
[10] R. J. Kline, M. D. Mcgehee, M. F. Toney, *Nat. Mater.* **2006**, *5*, 222.
[11] H. C. Yang, T. J. Shin, Z. N. Bao, C. Y. Ryu, *J. Polym. Sci, Part B: Polym. Phys.* **2007**, *45*, 1303.
[12] U. Jeng, C. H. Hsu, H. S. Sheu, H. Y. Lee, A. R. Inigo, H. C. Chiu, W. S. Fann, S. H. Chen, A. C. Su, T. L. Lin, K. Y. Peng, S. A. Chen, *Macromolecules* **2005**, *38*, 6566.
[13] T. Q. Nguyen, I. B. Martini, J. Liu, B. J. Schwartz, *J. Phys. Chem. B* **2000**, *104*, 237.
[14] H. E. Tseng, C. Y. Liu, S. A. Chen, *Appl. Phys. Lett.* **2006**, *88*, 042112.
[15] Y. F. Huang, A. R. Inigo, C. C. Chang, K. C. Li, C. T. Liang, C. W. Chang, T. S. Lim, S. H. Chen, J. D. White, U. S. Jeng, A. C. Su, Y. S. Huang, K. Y. Peng, S. A. Chen, W. W. Pai, C. H. Lin, L. R. Tameev, S. V. Novikov, A. V. Vannikov, W. S. Fann, *Adv. Funct. Mater.* **2007**, *17*, 2902.
[16] S. H. Chen, A. C. Su, H. L. Chou, K. Y. Peng, S. A. Chen, *Macromolecules* **2004**, *37*, 167.
[17] H. Yang, S. W. LeFevre, C. Y. Ryu, Z. Bao, *Appl. Phys. Lett.* **2007**, *90*, 172116.
[18] Parratt32 by C. Braun, free distribution by Hahn-Meitner-Institut, Berlin **1998**.
[19] C. Tanase, E. J. Meijer, P. W. M. Blom, D. M. de Leeuw, *Org. Electron.* **2003**, *4*, 33.
[20] L. J. A. Koster, V. D. Mihailetchi, P. W. M. Blom, *Appl. Phys. Lett.* **2006**, *88*, 093511.
[21] F. Wudl, G. Srdanov, US Patent No. 5189136, (**1990**).
[22] F. Wudl, G. Srdanov, *Chem. Abstr.* **1993**, *118*, 255575.
[23] M Bachman,, RCA-1 Silicon Wafer Cleaning, UCI Integrated Nanosystems Research Facility. Downloaded from http://www.ampel.ubc.ca/nanofab/sop/rca-clean-1.pdf. **1999**.
[24] D.-M. Smilgies, P. Busch, D. Posselt, C. M. Papadakis, In *Synchrotron Radiation News*, Vol. *15*, **2002**, p. 35.
[25] A. P. Hammersley, *ESRF Internal Report, *ESRF98HA01T*, FIT2D V9.129 Reference Manual V3.1* **1998**.